17th World Conference on Nondestructive Testing, 25-28 Oct 2008, Shanghai, China

Flaw Size Dependent Contrast Reduction and Additional Unsharpness by Scattered Radiation in Radiography

- Film and Digital Detectors in Comparison –

- Uwe EWERT, Uwe ZSCHERPEL, Carsten BELLON, Gerd-Rüdiger JAENISCH, Jörg BECKMANN, Mirko JECHOW

Institute for Materials Research and Testing (BAM), D-12200 Berlin, Germany;
Phone: +49 30 8104 1830, Fax: +49 30 8104 18 37;
E-mail: uwe.ewert@bam.de

Abstract

Radiographic image quality depends by its classical definition on contrast, noise (film: granularity as equivalent to noise) and unsharpness. These parameters are usually measured with image quality indicators (IQI). The scattered radiation reduces always the image quality in radiography. The different effects were analyzed to explain differences between applications of X-ray film, imaging plates (computed radiography) and digital detector arrays (DDA). In textbooks and standard guides (e.g. ASTM E1000) the scatter ratio k and different contrast definitions are given. This is for instance the radiographic contrast, specific contrast and the relative contrast. For digital media additional parameters are introduced as signal/noise ratio (SNR) and contrast/noise ratio (CNR), whereas the inverse CNR is the well known contrast sensitivity (CS), which is typically measured with IQIs. The optimum conditions for film replacement are investigated in the European project FilmFree. In this context the influence of the scattered radiation is investigated as it is generated by the object and in the detector and its cassettes or casings. X-ray modeling (Monte Carlo technique) is used to calculate separately the effect of primary radiation and scattered radiation leaving the object. Scattered radiation produced in the object and detector yields an image, which is the overlap of the projection by the primary radiation and a scatter image with higher unsharpness. This effect becomes dominant especially at higher radiation energies. Such scatter images are characterized by unsharpness values in the cm range. This disturbs classical radiography as well as digital radiography and computed tomography. Furthermore, an additional contrast reduction due to scatter effects is observed for small flaws, if the detector is in contact with the object. This effect depends on the flaw size and the distance between detector and object as well as the intermediate filtering.

Key words: Film, digital radiography, computed radiography, image quality, scattered radiation, scatter contrast, scatter unsharpness.

1. Introduction

The European Union is funding the project consortium “FilmFree” (http://www.filmfree.eu.com/) which supports the introduction of new technologies as Computed Radiography (CR) and Digital Detector Array (DDA) based radiography. These digital radiography techniques are now being applied to a broad range of X-ray applications, including inspection of pipeline welds, castings, electronic assemblies, wheels, rails, bridges and many other industrial uses for technical, environmental, safety and economic advantages. Increased emphasis on

environmental safety, including concerns for the effects of radiation on workers and the requirement for disposal of the chemicals used to process film, have contributed to the growing need to replace conventional X-ray inspections involving long film exposures. The relatively low operational cost of digital radiography and the possibility for online inspection are other major advantages of digital radiography. A consortium of thirty three partners, institutes, SMEs and large enterprises explores the application areas and the specific industry procedures for the application of CR and DDAs.

Computed Radiography (CR) and **D**igital **D**etectors **A**rray (DDA) systems were developed for medical applications, which have the potential to replace the X-ray film and revolutionize the radiological technique. These detectors enable new computer based applications with new intelligent computer based evaluation methods. These technological and algorithmic developments are also applicable to new NDT procedures.

The basic task of the project is the development of the correct procedure for industrial application. Some typical requirements for film application are invalid now. Most digital detectors are characterised by higher detector unsharpness than film. Lead screens do not intensify as much as in film radiography. The operator can use the digital detectors with much higher or lower exposure dose and achieve useful radiographs, but he can also make serious mistakes and spoil the image quality.

This study was carried out to determine the attenuation coefficients of the different detectors (film, imaging plates and digital detector arrays) and to find the contribution of scatter contrast and scatter unsharpness from the sample and detector environment.

2 Basics

The relative contrast C_r, which is mainly used for digital systems, is normalized to the signal intensity (grey values proportional to radiation dose) at a given area in the image (see ASTM E 1000)[1]:

$$C_r = \Delta I / I \qquad (1)$$

The grey values as well as the density difference increases with increasing exposure time (dose). For very small thickness changes (differential) it can be derived from the attenuation law (see ASTM E1000) with μ_{eff} (in 1/mm) as effective attenuation coefficient:

$$C = I \, \Delta w \, \mu_{eff} \qquad (2)$$

The specific contrast C_s (not relative specific contrast!) is now defined as detector response which is ΔI per thickness change (grey values per mm):

$$C_s = C/\Delta w = I \, \mu_{eff} \qquad (3)$$

Here, I is either the grey value of a specific pixel in a digital image or the optical density of a specific location at film. The grey value of a detector element is also considered as the signal of this detector element in response to a certain radiation dose. Therefore, the detector signal S for a given dose (if linear to dose) determines the contrast of a flaw or IQI in any radiographic image as follows:

$$C_s = S \, \mu_{eff} \qquad (4)$$

μ_{eff} is the effective attenuation coefficient which depends on the tube voltage, material and thickness of the object, tube filters, and detector screens as well as scattered radiation. The visibility of a certain flaw or IQI in an image depends not only on the C_s, it also depends on the image noise. Flaws and IQIs are only discernable if the contrast is higher than the image noise. Noise is caused by the fluctuations of the signal intensities of the different detector elements due to the quantum statistics and the different detector sensitivities. Wires and lines are visible if the contrast-to-noise ratio CNR is about one, pores and 1T holes are visible if CNR > 2.5. A higher exposure dose increases the CNR proportional to the square root of dose (or exposure time) due to the X-ray quantum statistics (Poisson distribution), if the detector responds linearly to dose and no other noise sources contribute to the image.

The contrast-to-noise ratio CNR, which is the essential parameter for the perception of flaws and IQIs, can be calculated from the detector response (SNR) as a function of signal and dose as follows (small flaws, see equation 3):

$$CNR/\Delta w = SNR \cdot \mu_{eff} \qquad (5)$$

Therefore, the image quality depends on the effective attenuation coefficient μ_{eff} and the detector response SNR. This applies for CR, DDAs and X-ray film. Fig. 1 illustrates the effect of noise.

The typical term for films is gradient-to-noise ratio (GNR). For NDT film systems it can be approximated by:

$$GNR \approx 2.3 \cdot SNR \qquad (6)$$

Since the grey values of the pixels in the digital images (if signal is linear to dose) depend on noise and signal intensity independently on the contrast and brightness processing for image viewing, the SNR has been proposed and accepted (EN 14784-1,-2 and ASTM E 2445, E2446) as an equivalence value to the optical density and a certain film system. The following discussion is based on this context.

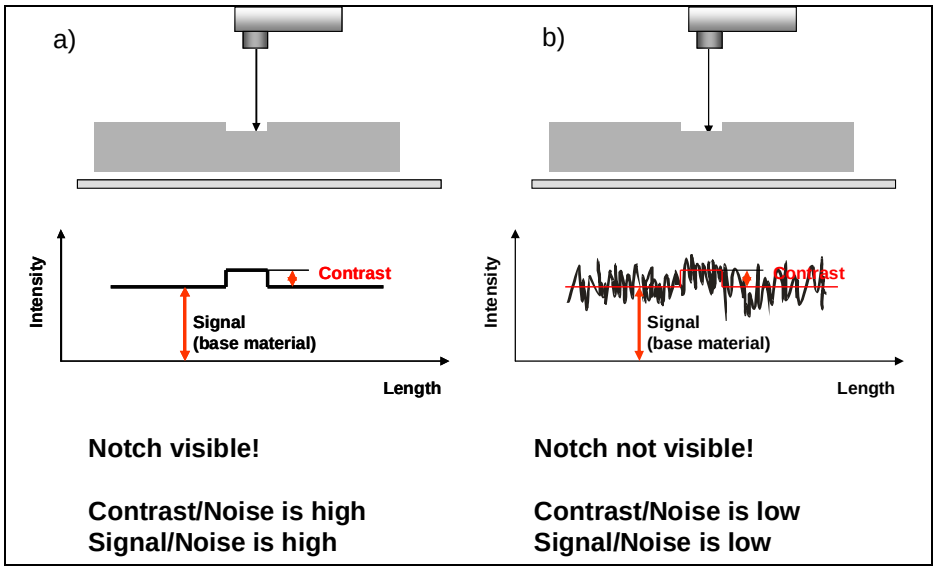

Fig. 1: Influence of noise on the visibility of a notch in radiography
a) the notch is visible if the noise contribution can be neglected,
b) the notch is not visible if the noise is about higher than the contrast.

Typically the operator determines in digital radiography the contrast resolution by the exposure time. Usually the image quality increases with the exposure dose[1-5] corresponding to equation 5. The SNR increases with exposure time, mA·s, GBq·min, 1/(source detector distance)² and the detector sensitivity (In case of valid Poisson statistics, SNR increases with square root of these parameters).

The image quality (contrast/noise ratio per wall thickness difference, which corresponds to the IQI visibility) increases also with increasing μ_{eff}. It depends on material, keV, radiating isotope, scattered radiation, screens, and filters. The following modelling and measurement procedures were performed to distinguish between scatter contributions and primary radiation contribution for steel inspection.

3 X-ray modelling by Monte Carlo ray tracer, coupled to CAD object description

3.1 Monte Carlo Model

The following assumptions are made to formulate the Monte Carlo model of photon transport: (*i*) the particles travel on a straight path between two interaction events without energy loss, (*ii*) one interaction per unit length occurs given by the linear attenuation cross section μ, (*iii*) the duration of an interaction is negligible compared to the time between two interactions. For photon transport three independent and mutually exclusive random events are considered: absorption τ, Compton scattering $\sigma_{Compton}$, and Rayleigh scattering $\sigma_{Rayleigh}$. The probability p_i of the collision event i is given by the ratio of the interaction cross section of the event i and the linear attenuation cross section μ: $p_1 = \tau/\mu$, $p_2 = \sigma_{Compton}/\mu$, $p_3 = \sigma_{Rayleigh}/\mu$.

The attenuation law determines the collision length l of a photon. Assuming piecewise constant material parameters the collision length is given by

$$l = -\frac{\ln \xi}{\mu} \tag{7}$$

with $\xi \in [0,1]$ being a uniformly distributed random number.

The implemented transport scheme consists of the three standard elements of Monte Carlo techniques: determination of (*i*) initial condition $(E_0,\mathbf{\Omega}_0)$, (*ii*) location of interaction from collision length l, and (*iii*) collision event i. If the photon leaves the object, no more interaction events are considered and the realization is terminated after registration in a detector element if hit. In case of an absorption event the realization is likewise finished. For a scattering event follows the determination of the new flight path direction and a possible energy loss $(E,\mathbf{\Omega}) \rightarrow (E',\mathbf{\Omega}')$, after which the scheme is repeated for the same realization from the second step until termination. The scheme is repeated until the preset number of realizations is traced or the required statistical accuracy is reached.

3.2 Object Description

In addition to the model of radiation transport, the radiographic simulation requires a virtual representation of the part or construction under testing. Unlike other Monte Carlo codes such as MCNP, an interface to CAD has been realized. Objects are described by closed surfaces separating regions of homogeneous material described by its attenuation properties. Several objects can be arranged in a virtual scene combined by simple Boolean operators forming complex parts. This realization also allows a flexible flaw generation and arbitrary positioning of flaws in complex parts.

The surface of an object is described by plane polygons allowing a simple mathematical treatment of a single polygon or facet. The size of the polygons is given by the local surface

curvature and the required accuracy of the surface approximation. The STL (stereo lithography) data format is used as exchange format for surfaces representation by triangles.

3.3 Monte Carlo Tracer

Primary and scattered photons are treated independently. The contribution of primary photons is calculated analytically from the attenuation law

$$I_p(\boldsymbol{r},\boldsymbol{\Omega},E) = I_0(\boldsymbol{r},\boldsymbol{\Omega},E)\, e^{-\int_0^{|\boldsymbol{r}-\boldsymbol{r}_0|} \mathrm{d}R\ \mu(\boldsymbol{r}-R\boldsymbol{\Omega},E)}. \tag{8}$$

Accordingly, only the scattered photons are traced by the Monte Carlo method. The probability for a surviving photon is given by $p_s = \mu_S / \mu$ with $\mu_S = \sigma_{Compton} + \sigma_{Rayleigh}$. This weight describes the average fraction of photons, which did not experience an absorption event. Accordingly, the surviving probability of a photon being scattered *n*-times follows as

$$p_s(n+1) = p_s(n)\frac{\mu_s(n+1)}{\mu(n+1)}. \tag{9}$$

This photon is registered with the weight given by eq. (9) at the detector plane if hit by elongating its path. It can formally be interpreted as an increase of the number of photon sources compared to the standard direct tracing of the photon's trajectory. Every following collision or scattering event decreases the photon weight and therefore its contribution final result. This treatment yields a reduction of variance in the result.

The described Monte Carlo algorithm has been implemented for parallel processing using MPI. The calculations discussed below are carried out on a Beowulf cluster built from standard PC components. It consists of a 4-processor server and 27 diskless nodes holding Pentium 4 core2 dual processor boards (in total 108 cores) with 1 GByte or 2 GByte memory per node. The nodes are booting the Linux kernel via network from the server.

The calculations presented here have been performed using 100 processors and a total number of photons traced of $1 \cdot 10^9$ (0.5 mm pixel size) and $1 \cdot 10^{11}$ (0.04 mm pixel size) resulting in statistical error for the scattered distribution of about 0.02 per pixel. The distance between the radiation source and the detector is 1000 mm assuming a monochromatic point source emitting photons at energy of 100 keV. The distance between the object and the detector has been chosen to be 0 mm, 5 mm, and 55 mm. As detector an ideal photon counter has been used.

4 Results of modelling for notch plates and its verification

Radiographs of different notch plates were calculated. A real notch plate was manufactured with notches of 0.03 mm to 2 mm width varying in depth from 0 to 3 mm (see fig 2). The notch plate is made from steel and was used to verify the modelling data.

4.1 Scatter contrast and scatter unsharpness

In most textbooks radiographic image quality parameters are restricted to contrast, noise (or granularity) and unsharpness.

The scatter contribution is typically explained by the build up factor B_{up} which considers the scatter ratio k as quotient of intensity of scattered radiation I_s to primary radiation I_p (see also ASTM E1000) with:

$$B_{up} = 1 + \frac{I_s}{I_p} = 1 + k \tag{10}$$

The simplified attenuation law is given by:

$$I = I_0 \cdot e^{-\mu \cdot w} \cdot B_{up} \tag{11}$$

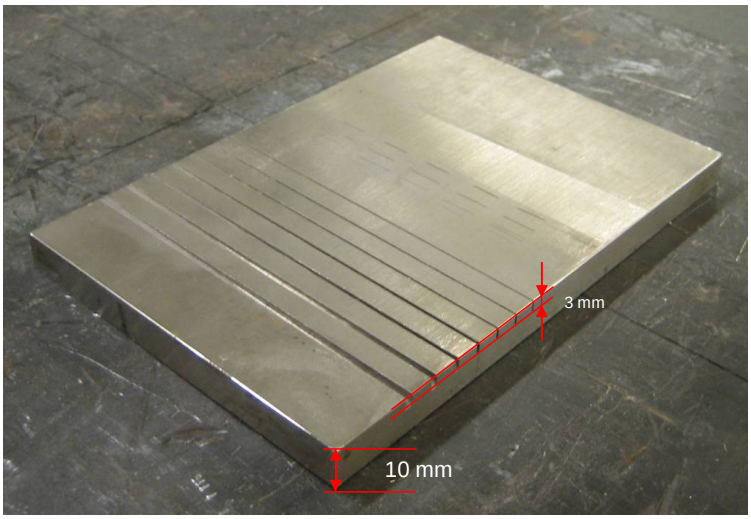

Fig. 2a: Notch plate of steel

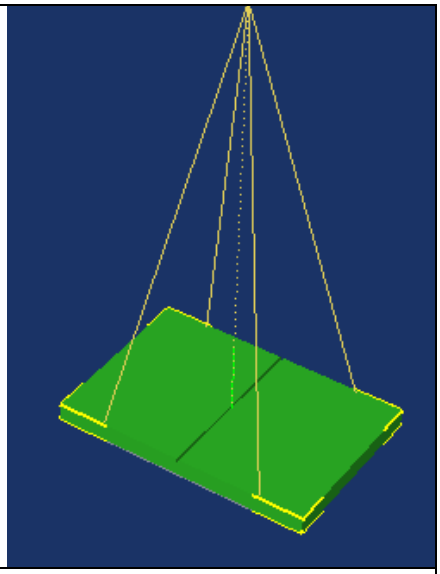

Fig. 2b: CAD-model of notch plate

The modelling software allows the separate calculation of primary radiation and scattered radiation. The goal of the study was the quantitative determination of the contribution of the scattered radiation. The results show a significant contrast enhancement due scattered radiation which depends on the notch width. The scatter image contributes to the total radiograph with additional scatter unsharpness. Fig. 3 shows the separated profiles generated by primary and scattered radiation for a detector in contact to the notch plate. The scatter image contributes to the wider notches with about 30% of the total image contrast. The contrast enhancement depends on the notch width and decreases with decreasing width of the notches. This effect leads to a variation of the radiation intensity behind notches of the same depth without any unsharpness contribution of the detector and geometrical unsharpness. The contrast of the fine flaws is reduced in relation to the larger ones, which has to be considered if digital tools are used to determine the flaw depth on the basis of a $\boldsymbol{\mu}$ calibration at large flaws, step wedges, flat bottom holes or plate IQIs.

The notch plate (fig. 2a) was used for verification of the modelling results. An imaging plate HD-IP was used as detector and an IP scanner HD-CR 35 NDT of Duerr to read the IP. The imaging plate (IP) was protected by a flexible polyethylene envelope without lead screens. All measurements were performed with a constant potential X-ray tube, Rich. Seifert & Co, AEG MB 450/1 (7 mm Be-Window), at 160 kV. The notch plate and IP was exactly positioned in 4 m distance to the x-ray tube to neglect the geometrical unsharpness. The IP was scanned with 21 µm pixel resolution of the Duerr scanner.

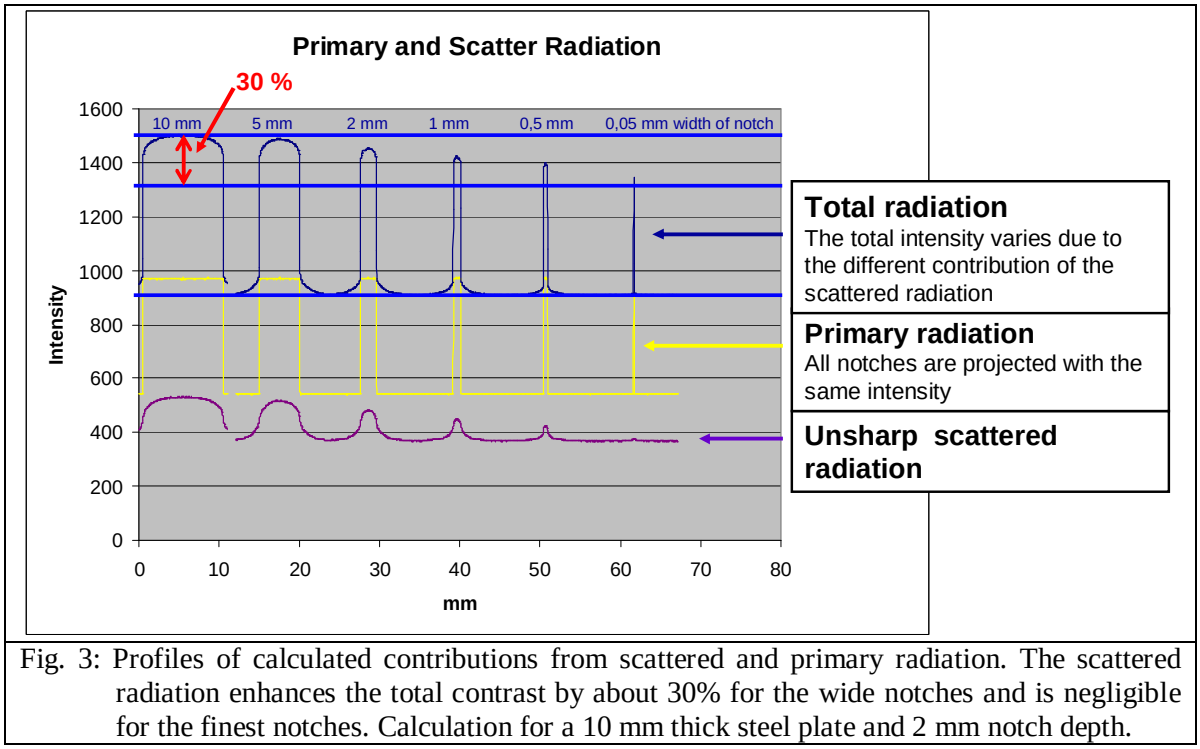

Fig. 3: Profiles of calculated contributions from scattered and primary radiation. The scattered radiation enhances the total contrast by about 30% for the wide notches and is negligible for the finest notches. Calculation for a 10 mm thick steel plate and 2 mm notch depth.

Fig. 4 shows the comparison of measured and calculated data. The unsharpness is visible in the curvature of the foot areas and as arc like shape in the top area of the notch profiles. The experimental and calculated data show sufficient agreement after normalisation to consider the IP sensitivity. The comparison was carried out for the 2 mm deep notch with 2 mm, 1 mm and 0.5 mm width. Fine notches with a width below 0.05 mm are not significantly enhanced by the scatter contrast. This means they appear in the radiograph with about 30% less contrast in comparison to the large flaws.

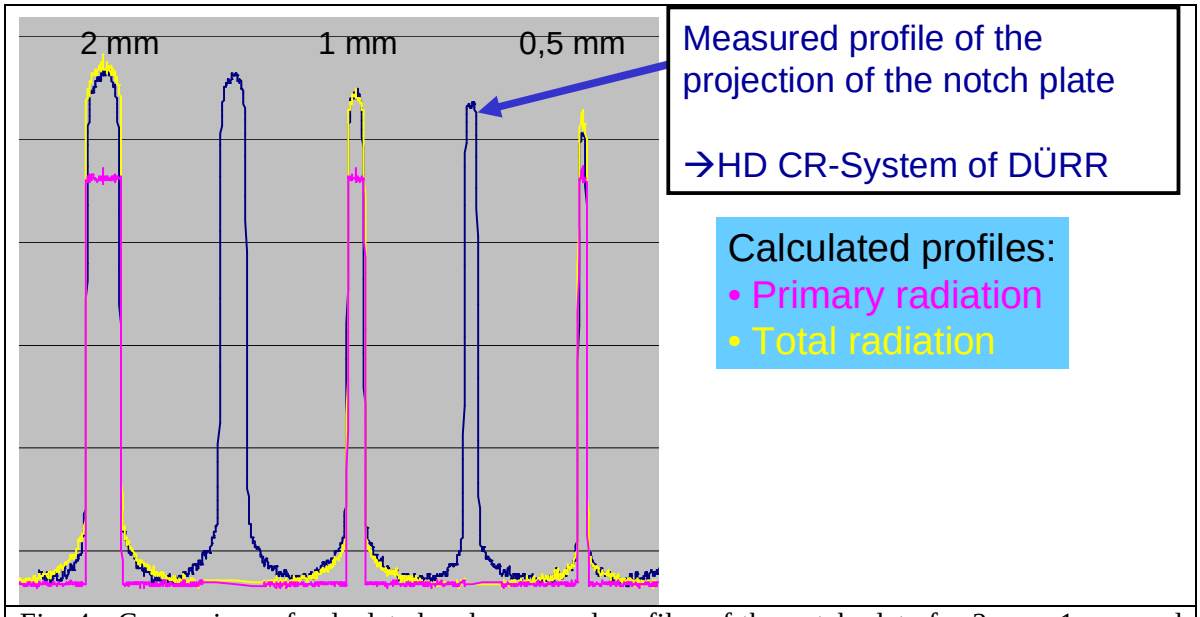

Fig. 4: Comparison of calculated and measured profiles of the notch plate for 2 mm, 1 mm and 0.5 mm wide and 2 mm deep notches.

The effect of additional scatter contrast and unsharpness depends on the distance between detector and object (see fig. 5). This effect was studied by modelling. The detector was

located in contact with the notch plate as well as in 5 and 55 mm distance to the plate. The distance between detector and object is typical for radioscopy, the usage of digital detector arrays (DDA) and computed tomography. A DDA is typically used in some distance to the object due to the dimension of the detector casing and for protection of the detector. Films and imaging plates are used in dependence on the cassette size in contact or in few mm distance, respectively. The observed change of scatter contrast has to be considered for the determination of the exposure time. For 5 mm and 55 mm distance a Hamamatsu C7940DA-02 was carefully positioned and calibrated by D. Fratzscher. He used a multi gain calibration to achieve the high contrast sensitivity mode, which was described earlier[2-4]. Fig. 5 shows the comparison between calculations and measurements. The experimental data were normalised differently to correct for the different sensitivity of DDA and IP.

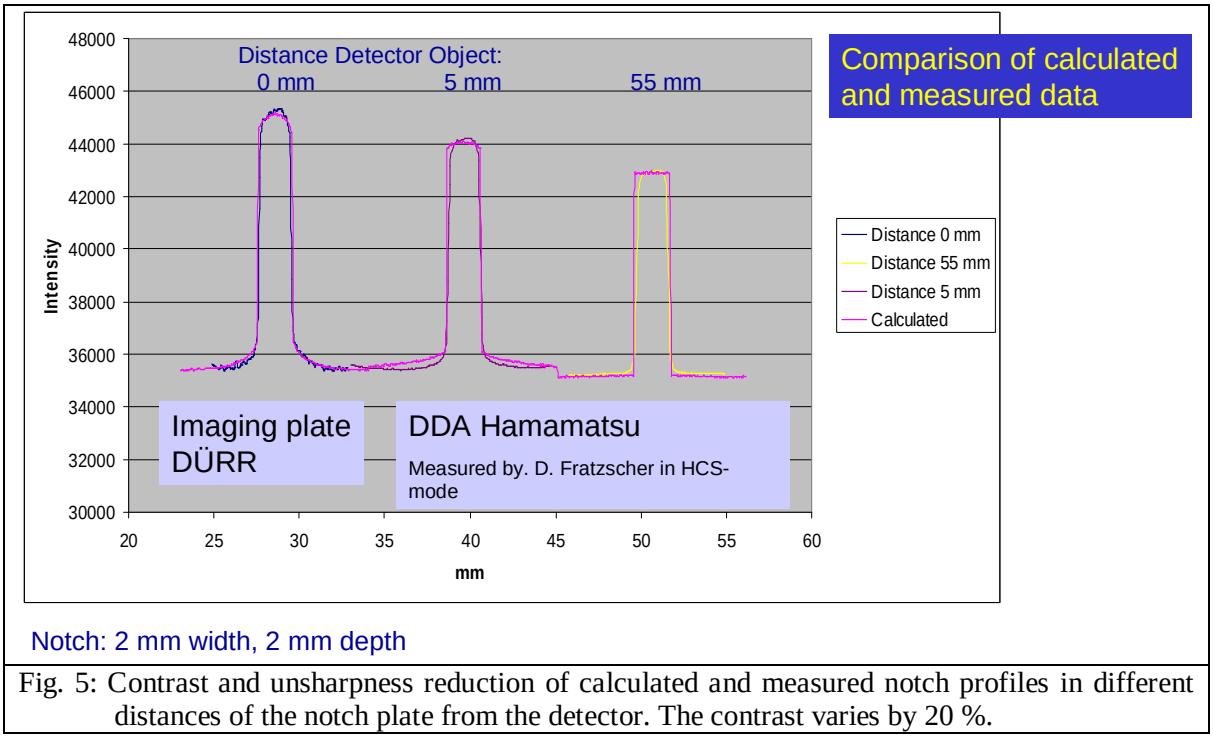

Fig. 5: Contrast and unsharpness reduction of calculated and measured notch profiles in different distances of the notch plate from the detector. The contrast varies by 20 %.

4.2 Variation of the effective attenuation coefficient in dependence on wall thickness

The notch plate was used as a representative test object for radiography of welds. In contrast, castings are characterized by wall thickness variations all over the object. Therefore, it is necessary to consider the change of the scatter ratio as function of the wall thickness. A step wedge (steel) was selected as representative test object. The scatter ratio depends on the wall thickness variation and the detector. It is influenced by the selection of intermediate and pre-filters and the applied screens; typically lead screens are used. The scatter ratio was measured for films and imaging plates in different cassettes and with different lead screens[9]. Fig 6 shows the results of the measurements. The Agfa film system C3 (D4, vacupac) shows an almost linear dependence on the wall thickness. The scatter ration was determined with $k \approx 0.06 \cdot w$ for a wall thickness range of 0 to 35 mm (see fig. 6 for exact values). Each k value in the graph of fig. 6 was determined for a certain wall thickness and the corresponding maximum X-ray kV-value for steel of fig. 1 in EN 444. The k-value depends dominantly on the wall thickness of steel and varies only in a small range with the X-ray energy. The increase of lead thickness of 0.1 mm front and back screens reduces the k values for film by about 15 %. All experiments were carried out here with the imaging plate ST-VI of FujiFilm and the XG1 reader of the same company. The data of the XG1 system were red with a home made software. The data analysis was carried out with the program ISee

(www.kb.bam.de/~alex/ic.html). The IP was placed in different cassettes and in a polyethylene envelope. The lowest scatter ratio was obtained for the Agfa cassette CR TOWER with 250 µm lead as front screen in contact and a backscatter protection of 150 µm lead behind the magnetic holder sheet in the cassette. The highest scatter ratio was obtained for the IP in a polyethylene envelop without any lead shielding. This means that imaging plates are much more sensitive against scattered radiation than film, if no additional lead shielding is used. This results in an increased contrast difference between large and fine flaws in comparison to film.

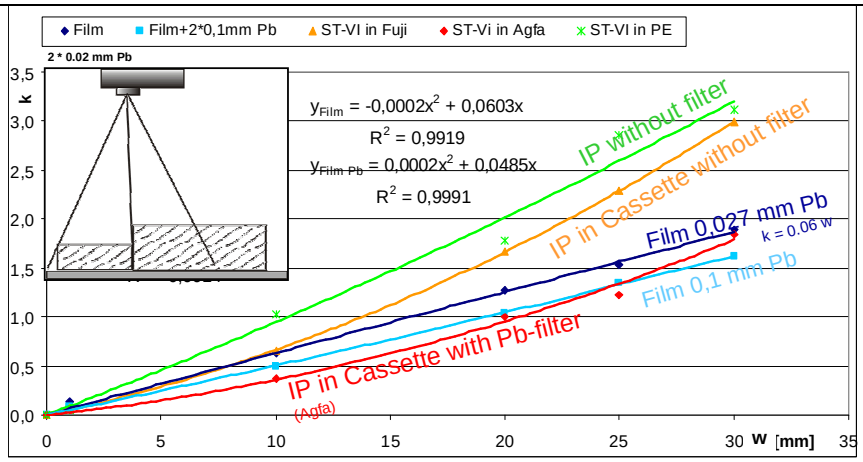

Fig. 6: Scatter ratio k as function of wall thickness and X-ray energy for X-ray films and imaging plates in different cassettes.

Front screens do not significantly intensify the radiographic image intensity of IPs, but they filter the scattered radiation. A side effect is an additional unsharpness due to scatter and X-ray fluorescence of lead. Lead back scatter filter contribute also to the image intensity due to scatter and X-ray fluorescence. The intensification of lead back screens or lead back filter plates amounts to about 40% at 220 kV. This intensification does not significantly contribute to contrast enhancement but increases image unsharpness. It is recommended to shield the IP with a steel or copper screen between lead and IP at the back side.

The k values were determined from step wedge exposures a) in contact with the detector and a source detector distance (SSD) of 1200 mm and b) in a distance of 600 mm from the detector (magnification of 2) for the same SDD. When shifting the step wedge towards the source, the total intensity I_{total} in the radiographic image decreases due to reduced intensity of scattered radiation from the step wedge. Finally in a distance of 600 mm between detector and object with the same SDD, the influence of the scattered radiation can be neglected; k is reduced to about zero and the total intensity is reduced to the intensity of primary radiation $I_{primary}$. The scatter ratio k for a certain wall thickness and X-ray energy is determined by:

$$k(w,E) = \frac{I_{total} - I_{primary}}{I_{primary}} \qquad (12)$$

If small wall thickness changes are considered (small flaws) the attenuation law is approximated corresponding to eq. 3 and the relative specific contrast for primary radiation is calculated:

$$C_{sp} = \mu_{eff} \qquad (13)$$

The calculation of the relative specific contrast depends now from the application considered. E.g. for butt weld inspection it is assumed that the wall thickness is about constant (ideal conditions). The flaw is an exception and it is always small. The build up factor is constant and the scattered radiation does not contribute to the flaw contrast. Eq. (14) in fig. 7a

describes (as typically published in text books) the contrast reduction of fine indications in dependence on the scatter ratio ($C_{sp1} = \mu_{eff1}$). No scatter protection leads to a significant drop of the specific contrast. This happens for steel dominantly above 10 mm (value may change depending on conditions) wall thickness, if the scatter filtering of lead screens compensates the hardening effect.

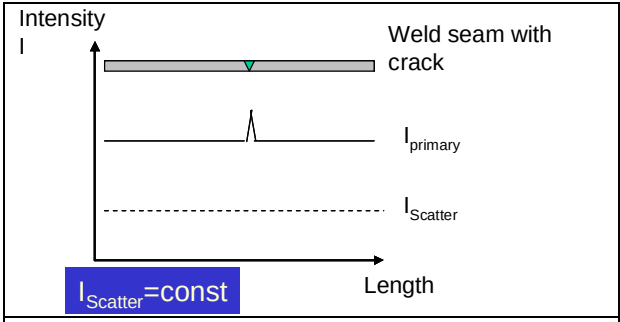

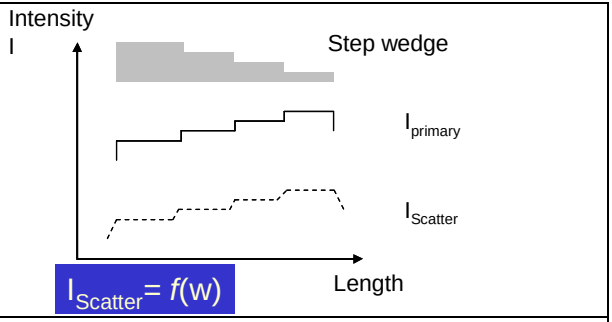

$$C_{sp1} = \frac{\mu_{primer}(w)}{1 + k(w)} \quad (14)$$

Fig. 7a: Model for calculation of the relative specific contrast 1 for fine flaws in welds.

$$C_{sp2} = \mu_{primer}(w) - \frac{1}{w} \cdot \ln(1 + k(w)) \quad (15)$$

Fig. 7b: Model for calculation of the relative specific contrast 2 for large flaws and castings.

For castings with a variety of different wall thicknesses eq. (14) is unsuitable, since the scattered radiation in contact technique contributes to the total contrast as proven above. Eq. (15) in fig. 7b shows the better description for calculation of the relative specific contrast, which corresponds to $C_{sp2} = \mu_{eff2}$, for different wall thicknesses and large flaws. Eq. (15) has been proven for the step wedge with the arrangement as shown in fig. 6. The edge unsharpness from scattered radiation of the object obtains several mm as shown in fig. 4.

5 Conclusion

The visibility of flaws and IQIs in digital radiology depends on the product of SNR in the radiographic image and the effective attenuation coefficient. The SNR depends on the quantum statistics and increases with increasing exposure time, and tube current or activity of a gamma source for a given SDD. The SNR saturates for CR and DDAs for high dose exposures. DDAs yield a higher SNR if properly calibrated[1,5].

Monte Carlo simulations were conducted to separate the contributions of primary and scattered radiation for a notch plate of steel to the total radiographic image. The scattered radiation generates an additional image, which is overlapped with the primary radiation image. The scatter image is unsharp and therefore the total image is characterised by a scatter unsharpness too. The simulated radiographs were successfully verified in comparison to real exposures with film, imaging plates and a DDA of a notch plate of steel.

The effective attenuation coefficient varies due to hardening and scattered radiation. The influence of scattered radiation was investigated with a step wedge and modelling. Imaging plates respond with higher scatter ratios than film with thin lead screens. Additional lead filtering (front screens) reduces the scatter ratio for imaging plates down to the film values. Lead screens do not intensify the IP images as in film radiography. Lead scatter and fluorescence contribute to additional unsharpness.

The effective attenuation coefficient, which can also be described as relative specific contrast, changes significantly in dependence on the flaw size. Two equations are derived (eq.

14, 15) to describe the contrast and effective attenuation coefficient of large and fine flaws separately.

Practitioners should consider that scattered radiation influences significantly the contrast of indications in dependence on the flaw size. For the steel notch plate of 10 mm thickness, contrast variations of 30 % due to scatter influences were determined for notches of different width.

6 References

[1] U. Ewert, U. Zscherpel, K. Bavendiek, Strategies for Film Replacement in Radiography - a comparative study -, PANNDT 2007, 22nd-26th Oct. 2007, Buenos Aires, Argentina, http://www.ndt.net/article/panndt2007/papers/142.pdf

[2] U. Ewert, BAM Berlin, U. Zscherpel, BAM Berlin, K. Bavendiek, YXLON International X-Ray, Hamburg, Digitale Radiologie in der ZfP - Belichtungszeit und Kontrastempfindlichkeit - Der Äquivalenzwert zur optischen Dichte des Films, DGZfP-Jahrestagung, Rostock, 2.-4.5.2005, Proceedings CD, v23.pdf and ZfP-Zeitung 97, 2005, S. 41 – 47.

[3] U. Zscherpel, BAM Berlin, U. Ewert, BAM Berlin, K. Bavendiek, YXLON International X-Ray, Hamburg, Bildschärfe digitaler radiologischer Detektoren für ZfP-Anwendungen, poster contribution, DGZfP-Jahrestagung, Rostock, 2.-4.5.2005 Proceedings CD, p38.pdf.

[4] U. Ewert, BAM Berlin, U. Zscherpel, BAM Berlin, K. Bavendiek, YXLON International X-Ray, Hamburg, REPLACEMENT OF FILM RADIOGRAPHY BY DIGITAL TECHNIQUES AND ENHANCEMENT OF IMAGE QUALITY, annual conference of Indian NDT society, Kalkutta, 4.-6.12.2005, V.S. Jain-Lecture, Proceedings, S. 3-15.

[5] Klaus BAVENDIEK, Uwe HEIKE, YXLON International, Hamburg, Germany, William D. MEADE, BOEING Commercial Airplane Group, Seattle, USA, Uwe ZSCHERPEL, Uwe EWERT, BAM, Berlin, Germany, New Digital Radiography Procedure Exceeds Film Sensitivity Considerably in Aerospace Applications, 9th ECNDT, Berlin, 25.-29.9.2006, Proceedings CD, Th.3.2.1.pdf (invited lecture).

[6] G.-R. Jaenisch, C. Bellon, M. Zhukovsky, and S. Podoliako:Numerical Simulation of X-Ray Scattering Process during Radiographic Inspection of Materials. The Russian Journal of NDT **42** 6, 382-391, 2006

[7] G.-R. Jaenisch, C. Bellon, U. Samadurau, M. Zhukovskiy, and S. Podoliako: Monte Carlo Radiographic Model with CAD-based Geometry Description. Insight **48** 10, 618-623 (2006)

[8] M. Zhukovsky, S. Podoliako, M. Skatchkov, and G.-R. Jaenisch: On Modelling Experiments with Ionizing Radiation (in Russian). Mathematical Modelling **19** 5, 72-80 (2007)

[9] A. Grosser, Optimization of image quality for imaging plates in NDT in dependence on the X-ray energy and steel thickness (in German). Diploma work (Reg. no.: P03/05/SS2007) at THF Wildau, Germany, 2007.